IAEA
International Atomic Energy Agency

20th IAEA Fusion Energy Conference
Vilamoura, Portugal, 1 to 6 November 2004

IAEA-CN-116/EX/P5-27

VARIATION OF PARTICLE CONTROL WITH CHANGES IN DIVERTOR GEOMETRY

T.W. PETRIE, S.L. ALLEN,[1] N.H. BROOKS, M.E. FENSTERMACHER,[1] J.R. FERRON, C.M. GREENFIELD, M. GROTH,[1] A.W. HYATT, A.W. LEONARD, T.C. LUCE, M.A. MAHDAVI, M. MURAKAMI,[2] G.D. PORTER,[1] M.E. RENSINK,[1] M.J. SCHAFFER, M.R. WADE,[2] J.G. WATKINS,[3] W.P. WEST, and N.S. WOLF[1]

General Atomics
San Diego, California 92186-5608
United States of America

[1]Lawrence Livermore National Laboratory, Livermore, California, USA
[2]Oak Ridge National Laboratory, Oak Ridge, Tennessee, USA
[3]Sandia National Laboratories, Albuquerque, New Mexico, USA

Variation of Particle Control with Changes in Divertor Geometry

T.W. Petrie, 1) S.L. Allen, 2) N.H. Brooks, 1) M.E. Fenstermacher, 2) J.R. Ferron, 1) C.M. Greenfield, 1) M. Groth, 2) A.W. Hyatt, 1) A.W. Leonard, 1) T.C. Luce, 1) M.A. Mahdavi, 1) M. Murakami, 3) G.D. Porter, 2) M.E. Rensink, 2) M.J. Schaffer, 1) M.R. Wade, 3) J.G. Watkins, 4) W.P. West, 1) and N.S. Wolf 2)

1) General Atomics, P.O. Box 85608, San Diego, California 92186-5608, USA
2) Lawrence Livermore National Laboratory, Livermore, California, USA
3) Oak Ridge National Laboratory, Oak Ridge, Tennessee, USA
4) Sandia National Laboratories, Albuquerque, New Mexico, USA

email: petrie@fusion.gat.com

Abstract. Recent experiments on DIII–D point to the importance of two factors in determining how effectively the deuterium particle inventory in a tokamak plasma can be controlled through pumping at the divertor target(s): (1) the divertor magnetic balance, i.e., the degree to which the divertor topology is single-null (SN) or double-null (DN), and (2) the direction of the of $B\times\nabla B$ ion drift with respect to the X-point(s). Changes in divertor magnetic balance near the DN shape have a much stronger effect on the particle exhaust rate at the inner divertor target(s) than on the particle exhaust rate at the outer divertor target(s). The particle exhaust rate for the DN shape is strongest at the outer strike point opposite the $B\times\nabla B$ ion particle drift direction. Our data suggests that the presence of $B\times\nabla B$ and $E\times B$ ion particle drifts in the scrapeoff layer (SOL) and divertors play an important role in the particle exhaust rates of DN and near-DN plasmas. Particle exhaust rates are shown to depend strongly on the edge (pedestal) density $n_{e,PED}$. In the lower range of densities considered in this study, i.e., $n_{e,PED}/n_{GREENWALD}$ <0.4, particle exhaust rates are also found to be approximately proportional to the deuterium recycling intensity in front of the respective plenum entrance. Our results are shown to have implications for particle control in ITER and other future tokamaks.

1. Introduction

Two important factors governing the attractiveness of the tokamaks are adequate plasma confinement time (τ_E) for plasma ignition and sufficiently high volume-averaged toroidal beta (β_T) for fusion power production [1]. Higher values of both τ_E and β_T are more readily obtained as the plasma shape becomes increasingly triangular, i.e., when the radial location of the X-point(s) are drawn closer to the tokamak centerpost. Higher overall triangularity is obtained only when the second point approaches the last closed flux surface defined by the first X-point, or as the single-null (SN) configuration approaches the double-null (DN) configuration. Because of the physics advantages of stronger shaping, it is important to evaluate and understand the discharge characteristics, as the SN configuration approaches the DN configuration.

A critical ingredient in the success of the DN concept is the degree to which the plasma density can be moderated or controlled. “Density control”, in turn, depends on how efficiently particles can be removed from the plasma system. Previous studies of unpumped DIII-D discharges have pointed toward two factors that could affect efficient particle removal. First, small variations in the magnetic balance near the DN shape have sizable effects on the poloidal distributions of heat and particle fluxes at the divertor targets [2,3], the edge localized mode (ELM)-driven particle pulses at the divertor targets [4], and the poloidal distribution of plasma recycling [5]. Second, ion particle drifts in the SOL and divertor(s), such as $B\times\nabla B$ and $E\times B$ drifts [6,7], contribute to the formation of poloidal “asymmetries” [8,9].

Magnetic balance and particle drifts, which play an important role in the plasma dynamics of *unpumped* divertor plasmas, may also provide the keys to understanding the dynamics of *actively pumped* ones [10]. We examined this hypothesis in a series of experiments at DIII-D during the 2003-2004 campaigns, with focus on DN and near-DN configurations. We describe the experimental setup in Section 2, present results in Section 3, and discuss these results in Section 4.

2. Experimental Arrangement

2.1. Plasma shape

Two types of DN and near-DN cross-sectional shapes were used in the study: *symmetric* and *non-symmetric*, depending on the radial positions R_{UP} and R_{DN} of the upper and lower X-points. For *symmetric* shapes, $R_{UP} \cong R_{DN}$. Three examples of symmetric poloidal cross-sections are shown in Fig. 1: (a) unbalanced upper DN, (b) balanced DN, and (c) unbalanced lower DN. In later discussion, we refer to the shapes in Fig. 1(a) and 1(c) as "upper SN" and "lower SN", respectively. Double-nulls and near-DNs are characterized as *non-symmetric* when $R_{UP} < R_{DN}$. Figure 2 shows a *non-symmetric* (but up-down magnetically balanced) DN. When the term *DN* is used without specification, the *symmetric* shape should be assumed. In either of the *symmetric* or the *non-symmetric* cases, note that both upper and lower X-points lie inside the vacuum vessel.

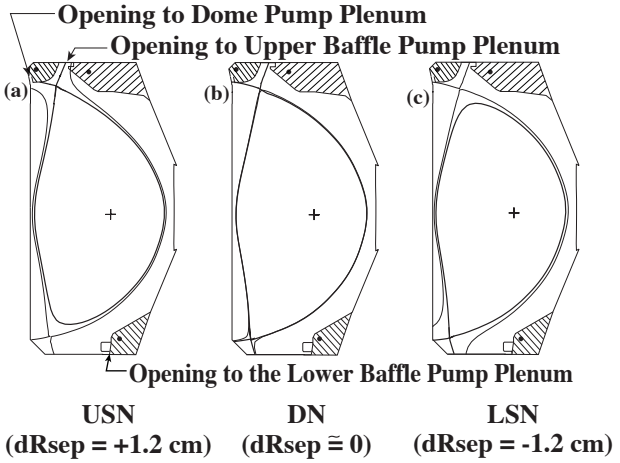

Fig. 1. Three types of symmetric equilibria used in this study: (a) DN biased toward the upper divertor ($dRsep$ = +1.2 cm), (b) balanced DN ($dRsep$ = 0), and (c) DN biased toward the lower divertor ($dRsep$ = -1.2 cm). The three cryo-ring pumps (solid circles) are located in the "dome", "upper baffle", and "lower baffle" plenums (cross-hatching), and they exhaust particles at the upper inner divertor target, at the upper outer divertor target, and at the lower outer divertor target, respectively. The lower baffle pump was not turned on during experiments with symmetric equilibria. The primary separatrix is shown as a heavy line; the secondary separatrix is shown as a lighter line.

To quantify the degree of divertor magnetic balance, we define the quantity $dRsep \equiv (R_L - R_U)$, where R_L is the radius at the outer midplane of the lower divertor separatrix flux surface and R_U the midplane radius of the upper separatrix flux surface. For example, for the upper SN case shown in Fig. 1(a), $R_U < R_L$ and $dRsep$ is positive.

2.2. Pumping configuration

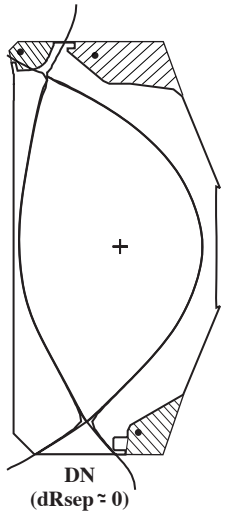

Fig. 2. A nonsymmetric DN configuration allows simultaneous particle pumping at three poloidal locations, as discussed in Sec. 2.2.

Active in-vessel pumping can be accomplished in DIII-D from three poloidal locations [11-14], as shown in Fig. 1. The cryo-ring pump located in the "dome" plenum exhausts particles from the upper inner divertor target; that in the upper baffle plenum exhausts particles from the upper outer divertor target. A third cryo-ring pump is located in the lower outer baffle plenum and exhausts particles from the lower divertor target, if the outer leg is nearby, as in the non-symmetric DN (Fig. 2). The rates at which particles are exhausted by the dome pump Γ_{DOME}, upper baffle pump $\Gamma_{UP\text{-}BAF}$, and lower baffle pump $\Gamma_{DN\text{-}BAF}$ are the respective products of the neutral pressure in their plenums and their pumping speeds S, where each S also depends weakly for these parameters on the plenum neutral pressure. Representative values of S for the dome and baffle pumps in these experiments were $\approx$17 m^3/s and $\approx$35-40 m^3/s, respectively.

Neutral pressure in each plenum is measured by a fast time-response ionization gauge [15]. Each gauge is located well away from the plenum entrance, so there is no path for direct line-of-flight energetic neutrals. Analysis shows multiple collisions of a deuterium neutral

with the plenum structure, leading to thermalization of the neutral inside the plenum, and the deuterium reaching the ionization gauge in molecular form.

2.3. General properties of the pumped plasmas

The plasmas used in this study exhibited Type-1 ELMing [16] and had good energy confinement, i.e., τ_E / τ_{E89P} = (2.1-2.5), where τ_{E89P} is the 1989 L-mode energy confinement scaling [17]. Plasmas are characterized by: I_p = 1.0-1.2 MA, $|B_T|$ = 1.85 T, q_{95} = 4.8-5.4, and $n_{e,PED} / n_{GREENWALD} < 0.4$, where $n_{e,PED}$ is the pedestal density and $n_{GREENWALD}$ is the Greenwald density [18]. Exhaust rates were measured for plasmas with the Bx∇B ion drift velocity directed either toward the upper divertor or toward the lower divertor, denoted hereafter by $V_{\nabla B\text{-UP}}$ and $V_{\nabla B\text{-DN}}$, respectively. Whenever possible, shots were repeated until the graphite armor which lines the vessel interiors was conditioned, such that successive shots were reproducible.

3. Experimental Results

3.1. Dependence of $\Gamma_{DOME}/\Gamma_{UP\text{-}BAF}$ on *dRsep*

Variation in the magnetic balance near DN in the symmetric cases affected the exhaust rates at the inner and outer divertor targets much differently. The ratio of inner to outer exhaust rates, $\Gamma_{DOME}/\Gamma_{UP\text{-}BAF}$, decreased steadily, as the magnetic balance changed from upper SN to lower SN (Fig. 3). This decrease was observed for *both* Bx∇B ion particle drift direction. The ratio of Γ_{DOME} to $\Gamma_{UP\text{-}BAF}$ decreased by roughly 2-3, as *dRsep* was lowered from +1 cm to zero, and decreased further as the plasma shape became lower SN (*dRsep* < 0).

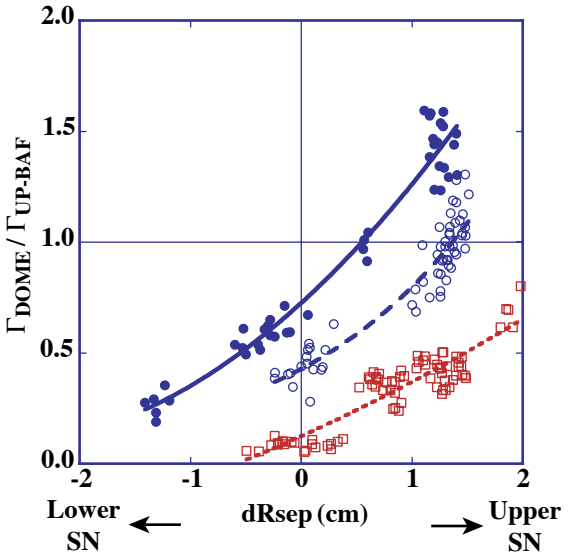

Fig. 3. The ratio $\Gamma_{DOME}/\Gamma_{UP\text{-}BAF}$ in symmetric plasma shapes varies with *dRsep* in the same manner for cases where the Bx∇B ion drift direction is toward the upper divertor (open diamonds and closed circles) and away from the upper divertor (open squares). Open diamonds are representative of data obtained during the 2002-2004 campaigns, and the closed circles indicate data obtained very early in the 2003 campaign. Characteristic parameters for these plasmas were: I_p = 1.2 MA, $|B_T|$ = 1.85 T, and P_{INJ} = 6-11 MW.

Figure 3 displays two different series of shots with $V_{\nabla B\text{-UP}}$ drift. The closed circles comprise a series of shots taken very early in the 2003 campaign; the open diamonds, a large set of data from the 2002-2004 campaigns. The differences in $\Gamma_{DOME}/\Gamma_{UP\text{-}BAF}$ likely reflects the length of exposure of he graphite armor tiles to high power ttokamak plasmas. Hence, the difference between these two cases reflects the variability of results under very different background conditions of the vessel.

3.2. Dependence of $\Gamma_{DOME}/\Gamma_{UP\text{-}BAF}$ on the Bx∇B ion particle drift direction

The ratio $\Gamma_{DOME}/\Gamma_{UP\text{-}BAF}$ was significantly different for the $V_{\nabla B\text{-UP}}$ and $V_{\nabla B\text{-DN}}$ cases. In the balanced DN case of Fig. 3, $\Gamma_{UP\text{-}BAF}$ was approximately a factor of eight times Γ_{DOME} for $V_{\nabla B\text{-DN}}$, but only 1.5-2.5 times Γ_{DOME} for $V_{\nabla B\text{-UP}}$. This result suggests that particle drifts in the SOL and divertor are playing a strong role in pumping dynamics, as we discuss in Sec. 4.2.

3.3. Dependence of Γ_{DOME} and $\Gamma_{UP\text{-}BAF}$ on pedestal density $n_{e,PED}$

Figures 4(a) and 4(b) show that Γ_{DOME} and $\Gamma_{UP\text{-}BAF}$ depend strongly on pedestal density $n_{e,PED}$, despite scatter in the data due to ELMs. After averaging $n_{e,PED}$ over several ELM periods, we find that: $(\Gamma_{DOME},\Gamma_{UP\text{-}BAF}) \propto [n_{e,PED}]^{(2.0\text{-}3.0)}$ in both upper the SN- and DN-

configurations. Thus, in any comparison of exhaust rates, it is important to account for the strong dependence on edge density.

3.4. Dependence of Γ_{DOME} and $\Gamma_{UP\text{-}BAF}$ on *dRsep*

The particle exhaust rates of discharges with $V_{\nabla B\text{-}DN}$ and $V_{\nabla B\text{-}UP}$ are compared in Fig. 5. Both DN discharges were virtually balanced DN (*dRsep* = 0) at *t* = 4.8 s [Fig. 5(a)] when their edge pedestal densities were comparable [Fig. 5(b)]. While Γ_{DOME} was comparable in these two shots near magnetic balance, $\Gamma_{UP\text{-}BAF}$ was about four times that of the $V_{\nabla B\text{-}DN}$ case.

A particle balance calculation is helpful in showing how Γ_{DOME} and $\Gamma_{UP\text{-}BAF}$ depend *individually* on *dRsep*:

$$0 = \Gamma_{INJ} - \Gamma_{DOME} - \Gamma_{UP\text{-}BAF} - \Gamma_{WALL} - dN_c/dt \quad , \qquad (1)$$

where (Γ_{INJ}) is the neutral beam fueling rate, (dN_c/dt) the rate that particles enter the plasma system (if positive), and (Γ_{WALL}) the rate that particles are lost (if positive) to the graphite tiles protecting the vessel walls, including the lower divertor. For cases where $V_{\nabla B\text{-}UP}$, Fig. 6 indicates that Γ_{DOME} was much more sensitive than $\Gamma_{UP\text{-}BAF}$ to small changes in magnetic balance near DN. For example, Γ_{DOME} dropped about a factor of two between *dRsep* = 0.0 cm and +1.2 cm, while $\Gamma_{UP\text{-}BAF}$ changed little.

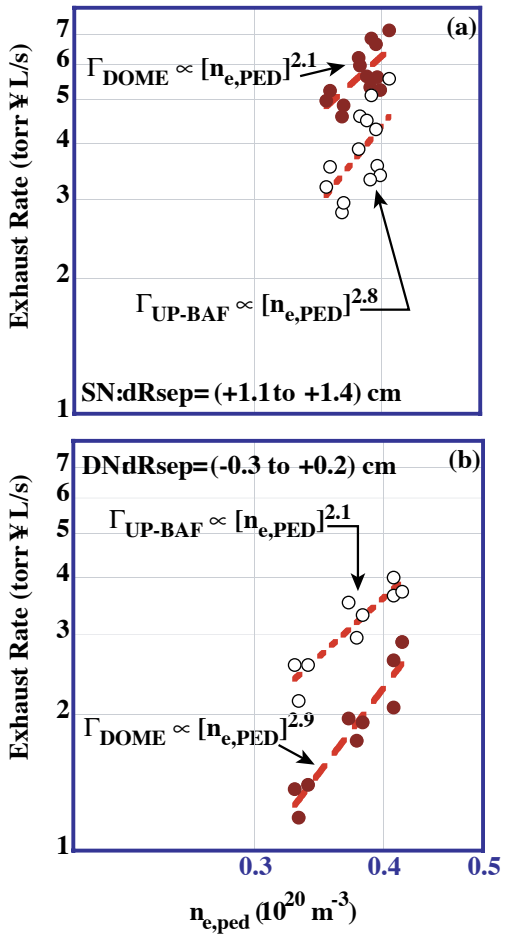

Fig. 4. $\Gamma_{UP\text{-}BAF}$ (open circles) and Γ_{DOME} closed circles) depend strongly on the pedestal density for both (a) SN cases with *dRsep* = (1.1-1.4) cm and the neutral beam fueling rate Γ_{INJ} = 13-5 torr liter/s, and (b) DN cases with *dRsep* = (-0.3-0.2) cm and Γ_{INJ} = 11-13 torr liter/s. The *B*x∇*B* ion particle drift was directed toward the upper divertor.

When the magnetic balance shifts from an upper SN to a balanced DN, the graphite armor "pumps" an increasingly higher fraction of the plasma exhaust at a fixed pedestal density. For *dRsep* ≃ +1.2 cm in Fig. 6, Γ_{WALL} was roughly one-third of the com-

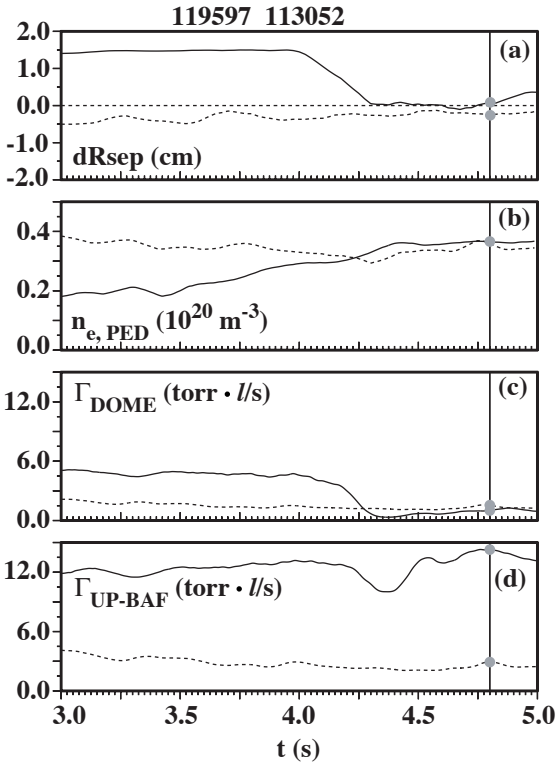

Fig. 5. Particle exhaust rates Γ_{DOME} and $\Gamma_{UP\text{-}BAF}$ are shown for $V_{\nabla B\text{-}DN}$ (solid) and $V_{\nabla B\text{-}UP}$ (dashed) in two similar symmetric DN discharges. The vertical line at t = 4.8 s denotes the time for comparison of the DNs.

bined dome and baffle pump rates ($\Gamma_{DOME} + \Gamma_{UP\text{-}BAF}$). In a well-conditioned vessel, "steady state" upper SN discharges could conceivably be maintained over several seconds under these conditions. However, as the configuration moves from the optimal upper SN toward DN and lower SN, wall pumping becomes a larger fraction of particle balance and partical control will become more difficult. A similar analysis was done for cases with $V_{\nabla B\text{-}DN}$. As with the $V_{\nabla B\text{-}UP}$ cases, Γ_{DOME} also showed a similar sensitivity to small changes in magnetic balance near DN, while $\Gamma_{UP\text{-}BAF}$ was again insensitive to change in *dRsep*.

3.5. Relationship between Γ_{DOME} and $\Gamma_{UP\text{-}BAF}$ and recycling activity

Changes in D_α recycling intensity in front of the entrance to a plenum is an indicator of changes occurring in the particle exhaust rate, and our experiments confirm this for the low density plasmas examined here. Figure 7 shows that for both (a) dome and (b) baffle cases, the number of particles exhausted by either the dome or baffle pumps is approximately proportional to the D_α recycling intensity (Φ) adjacent to their respective plenum entrances. In the case of the dome, e.g., $\Gamma_{DOME} \propto (\Phi_{DOME})^{1.05}$.

3.6. *Simultaneous* pumping of a non-symmetric DN at three poloidal locations

In the previous sections only the dome and upper baffle pumps were operating. In this section, we report pumping a DN plasma *with all three pumps operating*. Since it is not possible to pump a *symmetric* DN shape with the present pumping configuration in DIII-D, we have used a *non-symmetric* DN shape. We want to study the effect that particle drifts play when we pump the outer strike points of *both* divertors. However, because neither the plasma shape, the divertor structure, nor pumping characteristics are "up/down" symmetric, contributions to particle pumping from divertor geometry and plasma shape can "mask" the contributions from ion particle drifts.

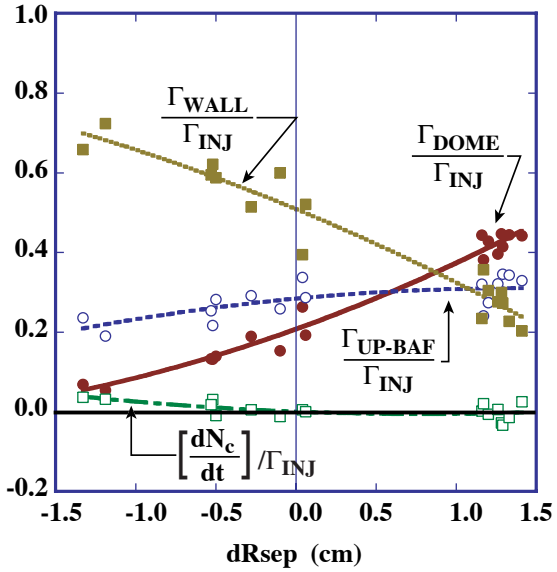

Fig. 6. The values of Γ_{DOME}, $\Gamma_{UP\text{-}BAF}$, and dN_c/dt were determined by measurement, while Γ_{WALL} was deduced from Eq. (1). These quantities are normalized to Γ_{INJ}. The data were characterized by $n_{e,PED}$ = 0.37-0.40x10^{20} Γ_{INJ} = 11-17 torr liter/s, and the Bx∇B ion particle drift direction was toward the upper divertor.

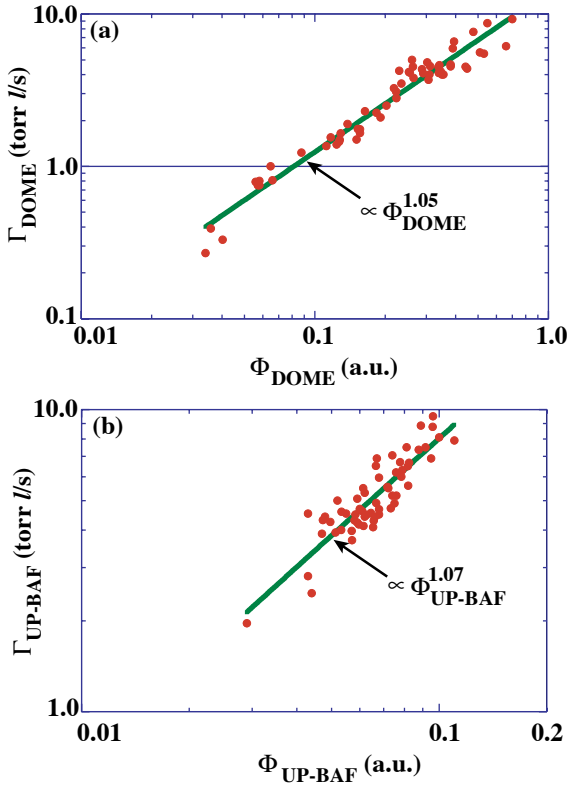

Fig. 7. (a) Γ_{DOME} and (b) $\Gamma_{UP\text{-}BAF}$ are plotted as a function of the D_α recycling radiation adjacent to the opening to their respective dome and baffle plenums, Φ_{DOME} and $\Phi_{UP\text{-}BAF}$, respectively. Data taken from $V_{\nabla B\text{-}UP}$ cases.

To alleviate this difficulty, we compare two high confinement, *identically shaped* non-symmetric DN plasmas, one with $V_{\nabla B\text{-UP}}$ and the other with $V_{\nabla B\text{-DN}}$ (Fig. 8). Both discharges achieved DN at t ≈ 4.24 s [Fig. 8(a)]. Since the edge (pedestal) density $n_{e,PED}$ was higher in the $V_{\nabla B\text{-DN}}$ case [Fig. 8(b)], both $\Gamma_{DN\text{-}BAF}$ and $\Gamma_{UP\text{-}BAF}$ have higher absolute values for the $V_{\nabla B\text{-DN}}$ case [Fig. 8(c) and (d)]. Although $\Gamma_{DN\text{-}BAF} > \Gamma_{UP\text{-}BAF}$ for both $V_{\nabla B\text{-DN}}$ and $V_{\nabla B\text{-UP}}$ cases, their ratio $\Gamma_{DN\text{-}BAF}/\Gamma_{UP\text{-}BAF}$ differed significantly: for $V_{\nabla B\text{-DN}}$, its value was ≈2.4 and for $V_{\nabla B\text{-UP}}$, its value was ≈5.2. That there is a difference in this ratio strongly again suggests that particle drifts in the SOL and divertors are present and that the exhaust rate at the outer target opposite the Bx∇B ion drift direction would be greater than at the other outer target of the DN, if both plasma shape and pumping configuration were actually up/down symmetric.

For both $V_{\nabla B\text{-DN}}$ and $V_{\nabla B\text{-UP}}$ cases, Γ_{DOME}, with a value of much less than 1 torr liter/s, is much smaller than $\Gamma_{DN\text{-}BAF}$ and $\Gamma_{UP\text{-}BAF}$ [Fig. 8(e)].

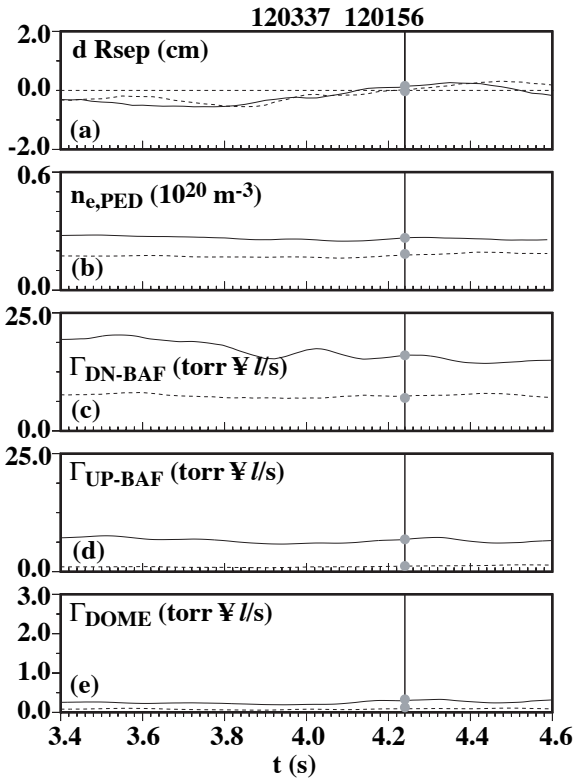

Fig. 8. Particle exhaust using all three pumps: A comparison of $\Gamma_{DN\text{-}BAF}$ and $\Gamma_{UP\text{-}BAF}$ for two similar non-symmetric DN discharges with $V_{\nabla B\text{-DN}}$ (solid) and $V_{\nabla B\text{-UP}}$ (dashed) is shown. Γ_{DOME} is also included. The timeslice of interest is t = 4.24 s. Characteristic parameters were: I_p = 1.0 MA, $|B_T|$ = 1.85 T, and P_{INJ} = 4 MW.

4. Discussion

4.1. Effects of magnetic balance

$\Gamma_{UP\text{-}BAF}$ was found to be much less sensitive than Γ_{DOME} to changes in *dRsep* near DN (Fig. 5). This result can be understood in terms of the number of particles entering the SOL from the "low-B_T" and "high-B_T" sides of the core plasma. This number is at least 3-4 times higher from the "low-B_T" side, due mainly to the larger plasma surface area and steeper radial density gradient on that side [2]. Also ELMing activity expels particles almost exclusively through the low-B_T side [4]. Consequently, particles that enter the SOL on the low-B_T side are the primary source of fueling for both the upper outer (baffle) target and the upper inner (dome) target, the latter through particles circulating poloidally in the SOL. Although the particle source from the high-B_T side is diminished when the magnetic balance shifts from upper SN to DN, this loss is a relatively minor effect on the total direct particle flow into the upper outer target (and, hence, the number of particles available for pumping). On the other hand, shifting the magnetic balance from upper SN to DN severs the direct route of particles from the low-field side, thus depriving the upper inner divertor of its major source of fueling (and reducing the number of particles available for pumping). Thus, changes in the magnetic balance near DN have a greater effect on Γ_{DOME} than on $\Gamma_{UP\text{-}BAF}$, which is relatively insensitive to changes in magnetic balance near *dRsep*=0. The above "geometric" argument applies in both $V_{\nabla B\text{-DN}}$ and $V_{\nabla B\text{-UP}}$ cases.

The above explanation assumes that the exhaust rate by each pump is proportional to the number of particles striking the divertor target (G_T) and that a geometrically-determined fraction of the neutrals "born" at or near the divertor target travel ballistically toward a plenum entrance without undergoing re-ionization enroute, i.e., the mean free path for ionization of these neutrals (λ_{ei}) is greater than the distance (D) from target to cryopump entrance

[19].This assumption is satisfied for the measured divertor densities typically $\approx 1.0 \times 10^{19}$ m^{-3}, we expect the particle exhaust rate to be proportional to G., e.g., $\Gamma_{DOME} \propto G_{DOME}$.

The strong dependence of Γ_{DOME} and $\Gamma_{UP\text{-}BAF}$ on pedestal density [Fig. 4(a,b)] can be understood in terms of the simple two-point model of the divertor, described in Ref. [20]. This model predicts that $G \propto (n_U)^2$ and $(n_{e,PED})^2$, where n_U is the "upstream" density in the SOL and n_U is firmly coupled to $n_{e,PED}$. From the discussion in the above, the strong dependence of Γ_{DOME} and $\Gamma_{UP\text{-}BAF}$ on pedestal density in Fig. 4 is expected.

The pumping rate and the recycling near a plenum entrance were shown to be linked by a near-linear relationship [Figs. 7(a),(b)]. The intensity of the recycling light near the entrances to the dome and upper baffle plenums (i.e., Φ_{DOME} and $\Phi_{UP\text{-}BAF}$, respectively) should be approximately proportional to the particle flux at the targets in front of their respective plenum entrances [20], e.g., $G_{DOME} \propto \Phi_{DOME}$. In turn, this leads to the observed result: $\Gamma_{DOME} \propto \Phi_{DOME}$ and $\Gamma_{UP\text{-}BAF} \propto \Phi_{UP\text{-}BAF}$.

4.2. Effect of particle drifts

Figures 5 and 6 show that changing the direction of the $B\times\nabla B$ ion drift has a pronounced effect on the ratio of Γ_{DOME} to $\Gamma_{UP\text{-}BAF}$. These exhaust rates for $V_{\nabla B\text{-}UP}$ and $V_{\nabla B\text{-}DN}$ cases which have the same *dRsep*, identical shape, identical divertor placement of the strike points relative to the pumping entrances, and the same pedestal density are quite different (Fig. 5). Detailed modeling of the pumped plasmas discussed in this paper is not complete. The indications are, however, that these differences are largely due to the presence of particle drifts in the SOL and divertor. Previous modeling of the SOL and divertor of *un*pumped, high triangularity DN plasmas using the 2-D fluid modeling edge transport code UEDGE [21] has shown that the observed asymmetries in the poloidal distributions of recycling radiation (or the neutrals available for pumping) were what would be expected if $B\times\nabla B$ and $E\times B$ ion particle drifts were present [4,5]. The electric field was mainly produced by the radial gradient of the electron temperature with respect to the flux surfaces in the private flux region (PFR) and the E direction is always away from the X-point. For instance, if the $B\times\nabla B$ ion drift direction was toward the upper divertor of the DN, UEDGE indicated that the $E\times B$ drift would transport ions through the PFR from the outer plate to the inner plate in the upper divertor, ultimately resulting in an enhanced recycling at that inboard plate. This process would be reversed for the lower divertor.

Figure 8 shows that changing the direction of the $B\times\nabla B$ ion drift affects the ratio of the exhaust rates between upper and lower *outer* divertor targets. As with the $\Gamma_{DOME}/\Gamma_{UP\text{-}BAF}$, UEDGE modeling has indicated that the observed higher D_α recycling at the outer divertor target opposite the $B\times\nabla B$ direction than at the other outer divertor target was also consistent with the presence of particle drifts, and one would expect higher exhaust rate in the former, if the pumping properties and the locations of the separatrix strike point relative to the plenum entrance are the same.

4.3. Some implications for particle control in ITER and other future tokamaks

For the *symmetric* DN and near-DN cases, only the dome and upper baffle pumps were active. This arrangement may be relevant to "high performance" ITER scenarios with sufficiently high triangularity. Such shaping is likely to lead to the formation of a secondary X-point *inside* the ITER vessel and, in turn, to the formation of a "passive" secondary divertor at the top of the vacuum vessel. Under these "finite *dRsep*" conditions, our data suggest that particle control for ITER would be only weakly affected, assuming that |*dRsep*| is maintained ≥1.5 cm and that the scrape-off widths in density and temperature are comparable to those in DIII–D. For the $B\times\nabla B$ ion drift toward the upper divertor, we found for *dRsep* = +1.2 cm the scrapeoff widths referenced to the outer DIII-D midplane of λ_{Te} = 0.6 cm and λ_{ne} = 1.2 cm , and λ_{Te} = 0.6 cm and λ_{ne} = 2.0 cm for the $B\times\nabla B$ ion drift away from the upper divertor.

For advanced tokamaks that have pumping capability in *both* divertors of a DN or near-DN shape, the data from our asymmetric DN experiment (Sec. 3.6) indicate that the exhaust rates at either of the *outer* divertor locations would be considerably greater than those at the *inner* divertor locations, and that pumping on the inner divertor leg would be of only marginal value in density control if both outer divertor pumps are operational. We also expect the particle exhaust rate to be higher at the outer divertor target *opposite* the $B\times\nabla B$ ion drift direction; for a pumping configuration similar to that of DIII-D, our analysis of the data in Sec. 3.6 indicates that the exhaust rate at the outer divertor target *opposite* the $B\times\nabla B$ ion drift direction is roughly 50% greater than that at the other outer divertor target. Additional studies of the pumping dynamics will be conducted in 2006, following modifications to the lower DIII-D divertor structure which will permit *simultaneous* pumping on the outer divertor legs of a *symmetric*, high performance DN plasma.

5. Conclusion

Two important considerations in understanding particle removal (and density control) in high confinement tokamak plasmas are: (1) the *magnetic balance* between divertor(s) and (2) the *directions of the particle drifts* in the SOL and divertor. Each of these considerations has been shown to generate sizable asymmetry in particle pumping between inner and outer divertor target(s) and between upper and lower outer divertor target(s).

Acknowledgment

This work was supported in part by the U.S. Department of Energy under DE-FC02-04ER54698, W-7405-ENG-48, DE-AC05-00OR22725, and DE-AC04-94AL85000.

References

[1] TAYLOR, T., Plasma Phys. and Contr. Fusion **39** (1997) 47.
[2] PETRIE, T.W., *et al.,* J. Nucl. Mater. **290-293** (2001) 935.
[3] PETRIE, T.W., *et al.,* Fusion Technol. **39** (2001) 916.
[4] PETRIE, T.W., *et al.,* Nucl. Fusion **43** (2003) 910.
[5] PETRIE, T.W., *et al.,* J. Nucl. Mater. **313-316** (2003) 834.
[6] CHANKIN, A.V., J. Nucl. Mater. **241-243** (1997) 199.
[7] BOEDO, J.A., *et al.,* Control. Fusion and Plasma Physics (Proc. Conf., Maastricht, 1999) Vol. 23J, European Physical Society (1999) 1185.
[8] ROGNLIEN, T.D., *et al.,* J. Nucl. Mater. **266-269** (1999) 654.
[9] RENSINK, M.E., *et al.,* Contrib. Plasma Phys. **42** (2002) 181.
[10] PETRIE, T.W., *et al.,* "Variation in Particle Pumping Due to Changes in Topology in High Performance DIII–D Plasmas" J. Nucl. Mater. (to be published).
[11] MAHDAVI, M.A., *et al.,* J. Nucl. Mater. **290-293** (2001) 905.
[12] ALLEN, S.L., *et al.,* J. Nucl. Mater. **266-269** (1999) 168.
[13] MAHDAVI, M.A., *et al.,* Fusion Engineering (Proc. Symp. Hyannis, 1993) Vol. 2, Institute of Electrical Electronics Engineers, Inc., Piscataway (1994) 597.
[14] MAINGI, R., *et al.,* Nucl. Fusion **44** (2004) 909.
[15] HAAS, G., BOSCH, H., Vacuum **51** (1998) 39.
[16] GOHIL, P., *et al.,* Phys. Rev. Lett. **61** (1988) 1603.
[17] YUSHMANOV, P.N., *et al.,* Nucl. Fusion **30** (1990) 1999.
[18] GREENWALD, M., *et al.,* Nucl. Fusion **28** (1988) 2199.
[19] MAINGI, R., *et al.,* Nucl. Fusion **39** (1999) 1187.
[20] STANGEBY, P.C., The Plasma Boundary of Magnetic Fusion Devices, Institute of Plasma Physics Publishing Ltd. (2000), Chapter 5.
[21] ROGNLIEN, T.D., *et al.,* Plasma Phys. **34** (1994) 362.